Unraveling the Homologation Reaction Sequence of the Zeolite-Catalyzed Ethanol-to-Hydrocarbons Process

Abhishek Dutta Chowdhury, Alessandra Lucini Paioni, Gareth T. Whiting, Donglong Fu, Marc Baldus, and Bert M. Weckhuysen*

Abstract: Although industrialized, the mechanism for catalytic upgrading of bioethanol over solid-acid catalysts (that is, the ethanol-to-hydrocarbons (ETH) reaction) has not yet been fully resolved. Moreover, mechanistic understanding of the ETH reaction relies heavily on its well-known "sister-reaction" the methanol-to-hydrocarbons (MTH) process. However, the MTH process possesses a C_1-entity reactant and cannot, therefore, shed any light on the homologation reaction sequence. The reaction and deactivation mechanism of the zeolite H-ZSM-5-catalyzed ETH process was elucidated using a combination of complementary solid-state NMR and operando UV/Vis diffuse reflectance spectroscopy, coupled with on-line mass spectrometry. This approach establishes the existence of a homologation reaction sequence through analysis of the pattern of the identified reactive and deactivated species. Furthermore, and in contrast to the MTH process, the deficiency of any olefinic-hydrocarbon pool species (that is, the olefin cycle) during the ETH process is also noted.

The production of (C_2–C_4) olefins is still primarily based on the cracking of natural gas and naphtha.[1,2] Since the direct carbon emissions from fossil feedstocks are considerably higher than for renewables, the economic and environmental motivations for replacement with renewables is steadily increasing every year.[1,3] For instance, ethylene is also currently manufactured from bioethanol-derived sugary and starchy feedstocks.[3–6] In fact, the ethanol-to-hydrocarbons (ETH) process carried out by catalytic upgrading over solid-acid catalysts has recently captured a lot of attention in academia[4–11] and industry.[3,6,12–14]

The ETH reaction was first commercialized by Elektrochemische Werke GmbH in Germany in 1913.[14] The supported phosphoric acid and activated alumina were used as a catalyst until the 1980s.[6,14] Zeolites were then introduced to achieve superior product selectivity and better environmental tolerance.[6,7,14] Despite these industrial advancements, the reaction and deactivation mechanisms of the ETH reaction are yet to be established. Moreover, mechanistic insights that are available to date are principally built on the understanding of the well-studied methanol-to-hydrocarbons (MTH) process.[2,15–17] This is because both ETH and MTH processes give similar product distributions.[18] However, it is not reasonable to assume that all zeolite-catalyzed conversion processes of alcohols would have an identical mechanism. A few exemplary characteristic differences are: 1) the MTH process requires a Koch-carbonylation-based direct mechanistic route to form the initial C−C bonds from C_1-methanol to produce ($\geq C_2$) products, which is apparently not needed from C_2-ethanol in the ETH process (Figure 1).[19–21] 2) It is impossible to evaluate the homologation reaction sequence during the MTH process, as all reaction products/intermediates are integers of its reactant C_1-methanol. Importantly, the ETH process offers us a unique possibility to investigate the homologation reaction in zeolite catalysis as it involves a C_2 reactant (Figure 1).

[*] Dr. A. D. Chowdhury, Dr. G. T. Whiting, D. Fu,
Prof. Dr. B. M. Weckhuysen
Inorganic Chemistry and Catalysis Group
Debye Institute for Nanomaterials Science
Utrecht University
Universiteitsweg 99, 3584 CG Utrecht (The Netherlands)
E-mail: b.m.weckhuysen@uu.nl

A. Lucini Paioni, Prof. Dr. M. Baldus
NMR Spectroscopy group, Bijvoet Center for Biomolecular Research
Utrecht University
Padualaan 8, 3584 CH Utrecht (The Netherlands)

Supporting information and the ORCID identification number(s) for the author(s) of this article can be found under:
https://doi.org/10.1002/anie.201814268.
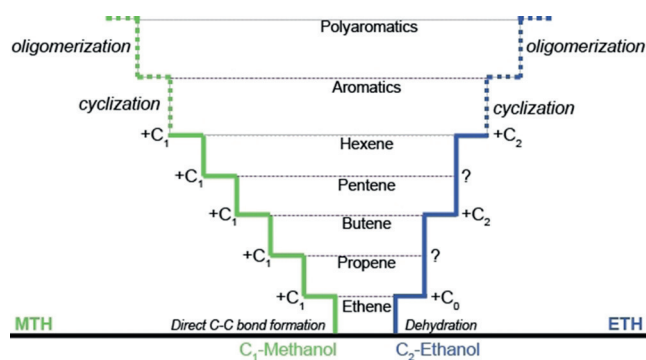
Figure 1. Simplified illustration of the alcohol homologation reaction sequence during zeolite-catalyzed MTH (in green) and ETH (in blue). Homologation is a reaction that increases the carbon skeleton of the reactant molecule to form the next higher analogues in multiples of *n*, where *n* is the number of carbon atom(s) in the reactant molecule (C_n; that is, $n = 1$ in MTH, $n = 2$ in ETH). Elucidation of the homologation reaction network and the origin of non-homologated products (marked as "?") during the ETH process forms the primary scope of this work. Dotted lines indicate the plausible existence of multiple steps.

These arguments collectively hint at the plausible existence of a different reaction mechanism occurring in the ETH process.

Only the first step of the ETH reaction (that is, dehydration) is relatively better understood in the literature.[8,22–25] Unfortunately, the rest of the reaction sequences (that is, homologation, cyclization, aromatization, and cracking) have yet to be unraveled. In particular, the exact mechanistic routes to the origin of $>C_2$ even-numbered (that is, homologated products such as C_4-butylene) and $>C_2$ odd-numbered (that is, non-homologated products such as C_3-propylene) carbon-containing hydrocarbon pool (HCP) species from C_2-ethanol are still under scrutiny within the ETH process. The importance of the mechanistic understanding of this industrial reaction should not be underestimated; as such, information is crucial to maximizing yields and developing new and/or improved heterogeneous catalysts.[26]

Aiming to dispel the ambiguity surrounding the zeolite-catalyzed ETH process, we have now established an in-depth fundamental mechanistic understanding of its complete reaction sequence—primarily by identification of multiple surface-adsorbed active catalytic species (that is, surface alkoxy and carbonylated species), C_2–C_4 olefins, homologated HCP (that is, hydrogen-transferred alkylated aromatics and smaller paraffin), and deactivated polyaromatic "coke" species. These new insights were obtained using advanced multidimensional magic angle spinning (MAS) solid-state NMR (ssNMR) spectroscopy, and corroborated with operando UV/Vis diffuse reflectance spectroscopy (DRS) coupled with on-line mass spectrometry (MS). In addition to the elucidation of the (homologation-dominated) reaction and deactivation mechanism, the mobility-dependent, distinctive host-guest chemistry between the zeolite and the trapped hydrocarbons during catalysis were also identified.[19,27,28]

Initially, operando UV/Vis DRS with on-line MS was used to identify and differentiate between neutral and carbocationic zeolite-trapped organic species, as well as gas-phase products, formed during an ETH reaction conducted at 573 K over millimeter-sized alumina-bound H-ZSM-5 extrudates (Figure 2; Supporting Information, Figure S1).[27] Figure 2a shows spectral features during the first 10 minutes of the reaction, as the absorption bands at ≤ 300, 336, 355, 421, and 576 nm increase in intensity as a function of reaction time (Figures 2b and 2c). The observed absorption bands at ≤ 300, 330–375, 421, and ≥ 575 nm are attributed to π–π* transitions associated with neutral alkylbenzene molecules, carbenium ions with alkyl side chain carbocations (up to four alkyl groups)/neutral polyaromatics, alkylated arenium molecules, and poly-arenium species/π-complexes between the zeolite and aromatic species, respectively (Supporting Information, Scheme S1).[8,19,27–29] Leveling off of the intensity of bands in the UV region after 7 minutes of reaction is indicative of the autocatalytic part of the reaction, whereas a continuous increase in the intensity of bands in the visible region indicates the formation of larger sized poly/fused aromatics (Figure 2c) during the deactivation of the catalyst.

The simultaneously measured on-line MS data reveal the predominant existence of diethyl ether and C_2–C_4 olefins (Figure S2d), along with C_4–C_7 hydrocarbon species in
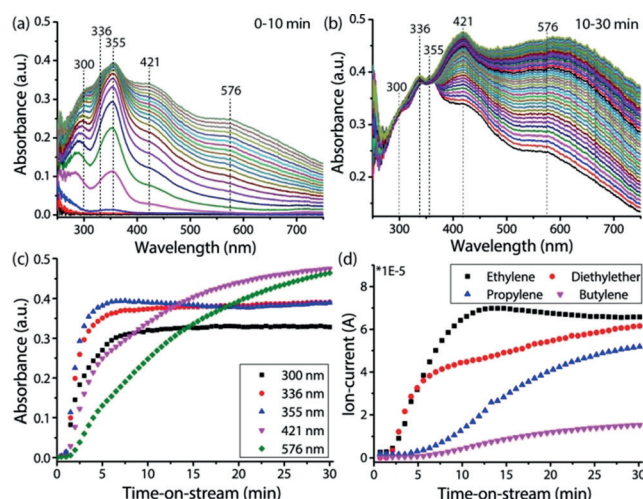

Figure 2. Operando UV/Vis DRS measurements during the ETH reaction over alumina-bound H-ZSM-5 extrudates at 573 K for a) 0–10 and b) 10–30 min. Time-resolved changes of c) absorbance bands and d) mass spectral profiles for diethyl ether and C_2–C_4 olefins as a function of reaction time.

relatively lower quantities (Figure S1b). Interestingly, no traces of $>C_8$ HCP species were detected in the effluent gas phase, whereas NMR could easily distinguish trapped $>C_{10}$ aromatic HCP species (see proceeding text). The simultaneous decrease and increase of ion current of ethylene and butylene (>10 min, Figure 2d), respectively, essentially demonstrates the ethanol-assisted dimerization of ethylene to butylene,[8] and hence, the existence of a homologation-reaction-mediated C–C bond-coupling sequence.

Advanced ssNMR was performed on the post-reacted material using $^{13}C_2$-labeled ethanol. The use of isotope-enriched ethanol not only significantly increased the NMR sensitivity, but also allowed us to perform multidimensional NMR correlation experiments for accurate structural determination of the homologation products. ^1H–^{13}C cross-polarization (CP),[30] ^1H–^{13}C insensitive nuclei enhanced by polarization transfer (INEPT),[31] and ^{13}C direct excitation (DE) ssNMR spectra show the following five features: 1) 7–37 ppm aliphatic groups, 2) 58–70 ppm alkoxy groups, 3) 125–160 ppm aromatic moieties, 4) 180–187 ppm carbonyl groups, and 5) additional peaks at approximately 227 ppm corresponding to carbocationic carbon nuclei (Supporting Information, Figure S2, Table S1). The strongest aliphatic and aromatic signals at 20–32 and 129–144 ppm, respectively, are mostly from the zeolite-trapped ethylated benzene molecules. This is consistent with the concept of both HCP species formation and the homologation reaction. The applied different NMR magnetization transfer techniques also allowed us to distinguish their spectral appearance on the basis of mobility.[19,27,28,32,33] As a result, both rigid (that is, physisorbed in/on zeolite; Figures 3 and 4; Figures S2–S9) and mobile (that is, with fast tumbling or local rotation; Figure S10) species of zeolite-trapped organics could be distinguished.

To probe the rigid molecules, 2D ^{13}C–^{13}C dipolar-based correlation spectra were acquired (Figures 3 and 4; Figures S2–S9).[34] In Figure 3a, we identified two non-identical
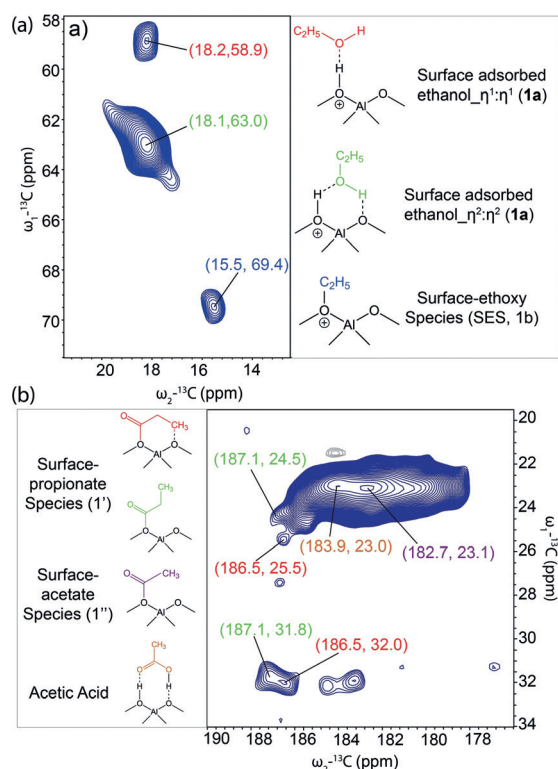
Figure 3. Magnification of the 2D MAS ssNMR spectra of rigid zeolite trapped molecules in the a) surface-adsorbed alkoxy and b) carbonyl regions. Spectra were recorded at 295 K, using 16 kHz MAS. Polarization of the ^{13}C atoms was achieved through CP and a 150 ms phase-alternated recoupling irradiation scheme (PARIS) mixing period was used.

binding motifs of the unreacted species, ethanol (**1a**), and the ethylating/homologation agent surface-ethoxy species (SES, **1b**). The peaks at 63.0 and 18.1 ppm corresponded to the methylene (-CH$_3$CH$_2$-) and methyl (-CH$_3$CH$_2$-) carbon (side-on, η^2:η^2) of ethanol, respectively.[27,35] In another spin system, a slightly upfield methylene carbon at 58.9 ppm, with an identical methyl chemical shift, was attributed to the end-on (that is, η^1:η^1) orientations of ethanol on the Brønsted acid site of H-ZSM-5.[27,35] We observed broader resonances for the "side-on" with respect to "end-on" conformation, indicating that the former exists in different molecular environments (that is, heterogeneity). Therefore, a "side-on" conformation of the ethanol adduct is more firmly adsorbed because of stronger H-bonding, which led to a downfield shift in the NMR signal.

In the carbonyl region, the correlations observed at 187.1/186.5 ppm exhibited cross-peaks with a ^{13}C-methylene signal at 31.8/32.0 ppm and another ^{13}C-methyl signal at 24.5/25.5 ppm, which corresponds to the surface-propionate (**1'**) species (Figure 3 b). Simultaneously, surface acetate (**1''**) (182.7/23.1 ppm, **1''**) and acetic acid (183.9/23.0 ppm; that is, the hydrolyzed product of **1''**), were also identified.[28] The presence of carbonylated surface species is consistent with the existence of the Koch-carbonylation-based direct C−C bond-forming route during the zeolite-catalyzed MTH process.[19–21,28]

To identify unique spin systems in the aromatic regions of rigid molecules, we collected ^{13}C–^{13}C correlation spectra using different mixing times (Figure S3). In the ^{13}C–^{13}C correlation spectrum with a short mixing time (30 ms), an intense cross-peak correlated a methyl resonance at 10.4 ppm with a resonance at 37 ppm (green cross in Figure 4). These
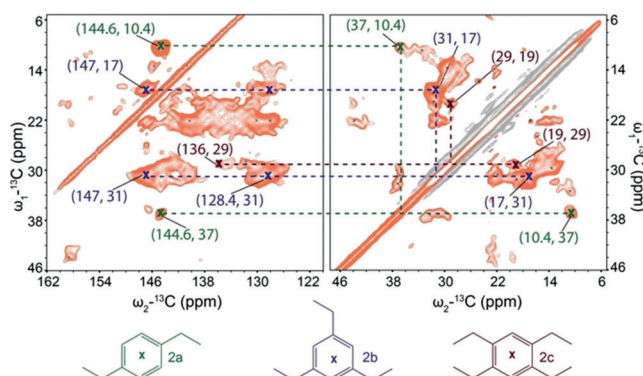

Figure 4. 2D ^{13}C–^{13}C ssNMR (16 kHz MAS) correlation experiments probing ethylated aromatics trapped by the rigid zeolite, measured at 295 K. Polarization of the ^{13}C atoms was achieved through CP and a 30 ms PARIS mixing period was used; spinning sideband (-----).

aliphatic resonances further correlated with aromatic carbon atoms through a strong peak at 144.6 ppm (green dotted line in Figure 4), which was assigned to diethylbenzene (**2a**). Similarly, tri- (**2b**, blue) and tetraethylbenzenes (**2c**, red) were also identified. In the experiment with a longer mixing time (120 ms), previous assigned correlations were confirmed and additional correlations were also identified; such as hexaethylbenzene (**2d**, Figure S4), multiple isomers of tetramethylbenzenes (**3a**; that is, isomerized from **2a**; Figure S7), and the two polyaromatic species tetraethylnaphthalene (**4a**) and hexahydropyrene (**4b**) (Figure S8). The identification of such homologated hydrocarbons (that is, **2a/2b/3a/4a/4b**) inside the post-reacted extrudate materials was further confirmed by so-called Guinset's method of zeolite-material dissolution (Figure S11, Section S1.5).[36]

Subsequently, weak signals at approximately 227 ppm in the 1D DE (Figure S2), and their cross-peaks with ^{13}C-methylene carbon atoms at 32–37 ppm in the ^{13}C–^{13}C correlation spectra (Figure S9), indicate the formation of alkylated carbenium species or a σ-complex within a six-membered ring framework.[16,27] Moreover, we detected mobile molecules (that is, ethanol and hydrogen-transferred C$_2$–C$_4$ alkanes; Figure S10) in 2D ssNMR experiments probing through-bond connectivities.[32]

Finally, a catalytic (homologation-dominated) reaction pathway for the ETH process is proposed in Scheme 1 (Scheme S2, Section S2). The first step involves dehydration of ethanol into ethylene, via a mono- or bimolecular pathway (with diethyl ether as an intermediate).[22] Firstly, ethanol is adsorbed on the zeolite through a H-bonding interaction with its Brønsted acid site (**1a**) with two binding motifs; that is, end-on (η^1:η^1) and side-on (η^2:η^2) conformations (Figure 3). Subsequently, **1a** undergoes dehydration over the zeolite to form SES (**1b**), followed by decomposition to eliminate
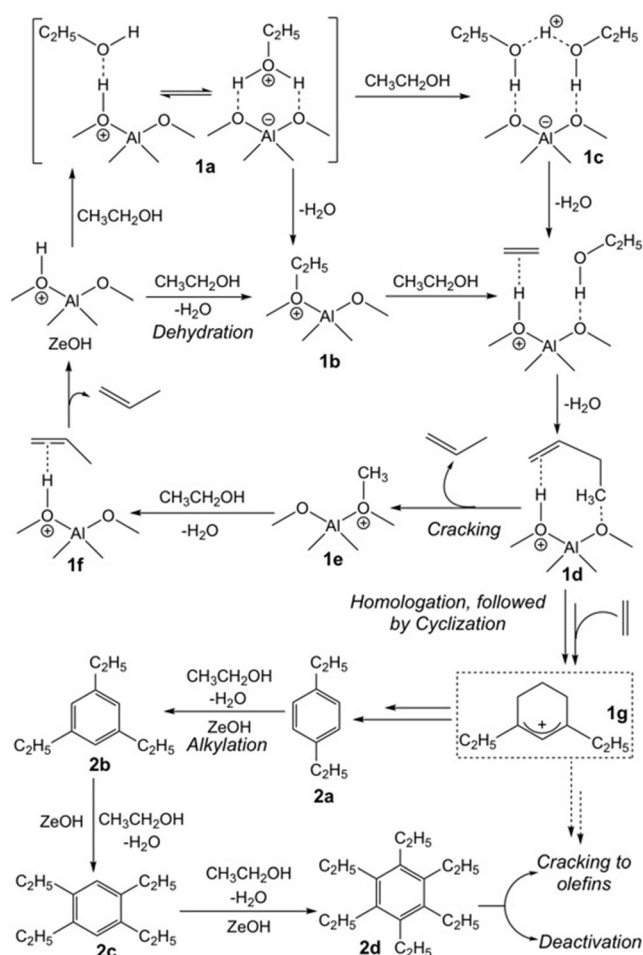
Scheme 1. Proposed mechanism for the homologation-reaction-dominated carbon–carbon bond coupling routes during the zeolite-catalyzed ETH process; plausible existence of multiple reaction steps (↔), the zeolite acid site (ZeOH).

ethylene and regenerate OH groups on zeolite via a concerted mechanism (monomolecular pathway, loop 1 in Scheme S2). The formation of ethylene from SES is concluded as the rate-determining step of the ETH process by Potter et al.[24] In a bimolecular pathway, the adsorption of another ethanol molecule on **1a** leads to the formation of a dimeric ethanol adduct on the surface of zeolite (**1c**), which is further decomposed/dehydrated to form diethyl ether and regenerates the zeolites in the process.[22]

Once the first ethylene forms from SES (**1b**), the homologation reaction is promptly initiated. Subsequently, ethanol undergoes the first homologation-reaction-mediated C–C bond coupling to form zeolite–butylene species (**1d**)—either directly from **1c** or when **1b** reacts with another ethanol molecule (Scheme 1). Species **1d** then directly generates either butylene and zeolite or propylene and surface-methoxy species (**1e**, as a result of cracking in Scheme 1). The first non-homologated product, propylene, is formed from surface-propylene species (**1f**) as a result of interaction between **1e** and ethanol. In the next stage, the homologation-reaction-mediated C–C bond-coupling route continues to dominate the ETH process. The species **1d** could

undergo further alkylation by ethanol and is followed by cyclization to form cyclic ethylated carbenium species (**1g**, Scheme 1). The cyclic **1g** species first led to a stable/neutral counterpart, diethylbenzene (**2a**) by dehydrocyclization, which reacts with ethanol/ethylene successively to produce a series of homologated products; that is, tri-/tetra-/hexa-ethylbenzenes (**2b–2d,** Scheme 1). Interestingly, most identified rigid ethylated aromatics have an even number of carbon atoms, which essentially advocates for the domination of the homologation-reaction-mediated C–C coupling routes during the ETH process.

The oligomerization/cyclization and isomerization of ethylated benzenes are two major deactivation pathways in the ETH process. The poly/fused-aromatic-based bulkier "coke" species (that is, **4a** and **4b** in Figure S8), are the primary deactivated species, which formed from ethylated benzenes through oligomerization via sequential C–H activation steps and followed by ring-closure (Scheme S2). These polyaromatic species are the precursor of pyrene (**4c**), which is a well-established, infamous coke/deactivated species in zeolite catalysis.[15,16,29,37,38] The methylated aromatics (that is, **3a** in Figure S7) were formed by cracking of bulkier species (compare **2d/4c**) and by isomerization from the ethylated aromatics (that is, **2a**) to tetramethylbenzene/durene (**3a**). Durene is an undesired side-product because of its high freezing point, and was not detected until now during the zeolite-catalyzed ETH process.[7] Simultaneously, Koch-carbonylated species (that is, surface-propionate (**1′**) and surface acetate (**1″**)) are independently capable of producing several methylated aromatic-based HCP species and C_2–C_4 olefins (Scheme S3).[19–21,28] Concurrently, C_2–C_4 alkanes (**5a–5c;** Figure S9) are formed as a result of the "concomitantly operating" hydrogen-transfer reactions from the corresponding olefins.[28]

In conclusion, our combined spectroscopic approach validates the hypothesis that the homologation-reaction-mediated C–C bond coupling is indeed responsible for the formation of olefins and its higher homologues during the zeolite-catalyzed ETH process. The "mechanistically decoupled" formation of ethylene from ethanol,[8] and its subsequent involvement in the formation of C_{3+}-HCP species (aromatics/alkanes) as a result of homologation reaction, govern both autocatalytic and deactivation segments of the reaction. Although the homologation-reaction-dominated HCP mechanism is found to be influential,[18] characteristically it is quite different from the MTH process because of the deficiency of its olefin cycle owing to its higher reactivity. The HCP species in the ETH process typically constitute multiple (m)ethylated aromatics (Table S3). Therefore, the acquired knowledge from this work will not only be useful for the development of superior materials for the catalytic upgrading of ethanol, but also contribute to the understanding of zeolite-catalyzed hydrocarbon conversion chemistry.

Conflict of interest

The authors declare no conflict of interest.

[1] M. Poliakoff, P. Licence, *Nature* **2007**, *450*, 810–812.

[2] I. Yarulina, A. D. Chowdhury, F. Meirer, B. M. Weckhuysen, J. Gascon, *Nat. Catal.* **2018**, *1*, 398–411.

[3] A. E. Farrell, R. J. Plevin, B. T. Turner, A. D. Jones, M. O'Hare, D. M. Kammen, *Science* **2006**, *311*, 506–508.

[4] A. Mohsenzadeh, A. Zamani, M. J. Taherzadeh, *ChemBioEng Rev.* **2017**, *4*, 75–91.

[5] C. Angelici, B. M. Weckhuysen, P. C. A. Bruijnincx, *ChemSusChem* **2013**, *6*, 1595–1614.

[6] M. Zhang, Y. Yu, *Ind. Eng. Chem. Res.* **2013**, *52*, 9505–9514.

[7] J. Sun, Y. Wang, *ACS Catal.* **2014**, *4*, 1078–1090.

[8] K. Van der Borght, R. Batchu, V. V. Galvita, K. Alexopoulos, M.-F. Reyniers, J. W. Thybaut, G. B. Marin, *Angew. Chem. Int. Ed.* **2016**, *55*, 12817–12821; *Angew. Chem.* **2016**, *128*, 13009–13013.

[9] K. Van der Borght, V. V. Galvita, G. B. Marin, *Appl. Catal. A* **2015**, *492*, 117–126.

[10] K. K. Ramasamy, M. A. Gerber, M. Flake, H. Zhang, Y. Wang, *Green Chem.* **2014**, *16*, 748–760.

[11] C. K. Narula, Z. Li, E. M. Casbeer, R. A. Geiger, M. Moses-Debusk, M. Keller, M. V. Buchanan, B. H. Davison, *Sci. Rep.* **2015**, *5*, 16039.

[12] "Solvay SA, Process for the Manufacture of Ethylene by Dehydration of Ethanol": EP 2594546, **2011**.

[13] "Catalytic Dehydration of Alcohols Using Phase Pure, Calcined Single- and Multi-Site Heterogeneous Catalysts": M. Lefenfeld, R. Raja, A. J. Paterson, M. E. Potter, US 8759599, **2010**.

[14] P. L. de Andrade Coutinho, A. T. Morita, L. F. Cassinelli, A. Morschbacker, R. Werneck Do Carmo in *Catalytic Process Development for Renewable Materials* (Eds.: P. Imhof, J. C. van der Waal), Wiley-VCH, Weinheim, **2013**, pp. 149–165.

[15] P. Tian, Y. Wei, M. Ye, Z. Liu, *ACS Catal.* **2015**, *5*, 1922–1938.

[16] U. Olsbye, S. Svelle, K. P. Lillerud, Z. H. Wei, Y. Y. Chen, J. F. Li, J. G. Wang, W. B. Fan, *Chem. Soc. Rev.* **2015**, *44*, 7155–7176.

[17] H. Schulz, *Catal. Lett.* **2018**, *148*, 1263–1280.

[18] R. Johansson, S. L. Hruby, J. Rass-Hansen, C. H. Christensen, *Catal. Lett.* **2009**, *127*, 1–6.

[19] A. D. Chowdhury, K. Houben, G. T. Whiting, M. Mokhtar, A. M. Asiri, S. A. Al-Thabaiti, M. Baldus, B. M. Weckhuysen, *Angew. Chem. Int. Ed.* **2016**, *55*, 15840–15845; *Angew. Chem.* **2016**, *128*, 16072–16077.

[20] P. N. Plessow, F. Studt, *ACS Catal.* **2017**, *7*, 7987–7994.

[21] Y. Liu, S. Müller, D. Berger, J. Jelic, K. Reuter, M. Tonigold, M. Sanchez-Sanchez, J. A. Lercher, *Angew. Chem. Int. Ed.* **2016**, *55*, 5723–5726; *Angew. Chem.* **2016**, *128*, 5817–5820.

[22] J. F. DeWilde, H. Chiang, D. A. Hickman, C. R. Ho, A. Bhan, *ACS Catal.* **2013**, *3*, 798–807.

[23] J. N. Kondo, H. Yamazaki, R. Osuga, T. Yokoi, T. Tatsumi, *J. Phys. Chem. Lett.* **2015**, *6*, 2243–2246.

[24] M. E. Potter, S. V. Aswegen, E. K. Gibson, I. P. Silverwood, R. Raja, A. Methivier, C. Ehlers, B. Farago, W. Haeussler, D. M. Ruthven, *Phys. Chem. Chem. Phys.* **2016**, *18*, 17303–17310.

[25] W. Wang, J. Jiao, Y. Jiang, S. S. Ray, M. Hunger, *ChemPhysChem* **2005**, *6*, 1467–1469.

[26] R. Ye, J. Zhao, B. B. Wickemeyer, F. D. Toste, G. A. Somorjai, *Nat. Catal.* **2018**, *1*, 318–325.

[27] A. D. Chowdhury, K. Houben, G. T. Whiting, S.-H. Chung, M. Baldus, B. M. Weckhuysen, *Nat. Catal.* **2018**, *1*, 23–31.

[28] A. Dutta Chowdhury, A. Lucini Paioni, G. T. Whiting, K. Houben, M. Baldus, B. M. Weckhuysen, *Angew. Chem. Int. Ed.* **2018**, *57*, 8095–8099; *Angew. Chem.* **2018**, *130*, 8227–8231.

[29] M. J. Wulfers, F. C. Jentoft, *ACS Catal.* **2014**, *4*, 3521–3532.

[30] A. Pines, M. G. Gibby, J. S. Waugh, *J. Chem. Phys.* **1973**, *59*, 569–590.

[31] G. A. Morris, R. Freeman, *J. Am. Chem. Soc.* **1979**, *101*, 760–762.

[32] O. C. Andronesi, S. Becker, K. Seidel, H. Heise, H. S. Young, M. Baldus, *J. Am. Chem. Soc.* **2005**, *127*, 12965–12974.

[33] Z. Ristanović, A. D. Chowdhury, R. Y. Brogaard, K. Houben, M. Baldus, J. Hofkens, M. B. J. Roeffaers, B. M. Weckhuysen, *J. Am. Chem. Soc.* **2018**, *140*, 14195–14205.

[34] M. Weingarth, D. E. Demco, G. Bodenhausen, P. Tekely, *Chem. Phys. Lett.* **2009**, *469*, 342–348.

[35] W. Wang, M. Seiler, M. Hunger, *J. Phys. Chem. B* **2001**, *105*, 12553–12558.

[36] M. Guisnet, *J. Mol. Catal. A* **2002**, *182–183*, 367–382.

[37] E. Borodina, F. Meirer, I. Lezcano-Gonzalez, M. Mokhtar, A. M. Asiri, S. A. Al-Thabaiti, S. N. Basahel, J. Ruiz-Martinez, B. M. Weckhuysen, *ACS Catal.* **2015**, *5*, 992–1003.

[38] J. Goetze, F. Meirer, I. Yarulina, J. Gascon, F. Kapteijn, J. Ruiz-Martínez, B. M. Weckhuysen, *ACS Catal.* **2017**, *7*, 4033–4046.